Unstable Polymer Bilayers. 2. The Effect of Film Thickness

4 **AUTHORS**, INCLUDING:

Karen I Winey
University of Pennsylvania
331 PUBLICATIONS **11,306** CITATIONS

SEE PROFILE

Russell J Composto
University of Pennsylvania
117 PUBLICATIONS **1,778** CITATIONS

SEE PROFILE

Unstable Polymer Bilayers. 2. The Effect of Film Thickness

Qi Pan,[†] Karen I. Winey,[†] Howard H. Hu,[‡] and Russell J. Composto*,[†]

Department of Materials Science and Engineering and Laboratory for Research on the Structure of Matter, University of Pennsylvania, Philadelphia, Pennsylvania 19104-6272, and Department of Mechanical Engineering and Applied Mechanics, University of Pennsylvania, Philadelphia, Pennsylvania 19104

The dewetting of a polycarbonate (PC) film from a poly(styrene-*co*-acrylonitrile) (SAN) film on a silicon substrate is studied at 180 °C, a temperature above the glass transition temperatures of PC and SAN. The viscosity ratio of PC to SAN is ~10. Using optical microscopy and video image analysis, the hole diameter D is measured at SAN layer thicknesses L from 125 to 1850 nm. For a PC thickness H of 200 nm, D varies linearly with time, which signifies a constant hole velocity. Initially, the hole velocity increases linearly with L and then becomes nearly constant for $L > 1000$ nm, which is the dissipation depth. Atomic force microscopy (AFM) studies show that the SAN thickness inside the hole is less than the original L. Analysis of the hydrostatic and dynamic pressures acting on the SAN inside and outside the hole is used to explain this result. For a very thin SAN film (i.e., $L \sim 50$ nm), D initially increases quickly with time, slows down, and then increases again. Using AFM, the retarded intermediate growth stage is shown to coincide with hole impingement on the silicon substrate. With an increase of H to 310 nm, D is found to accelerate with time. As L decreases from 1850 to 125 nm, the power law exponent ranges from $x = 1.1$ to 1.6, where $D \sim t^x$. A cross-sectional transmission electron image of the three-phase boundary shows that SAN is pulled into the rim in contrast to simple dewetting assumptions. Using the measured shape of the rim, the flow field within the rim is calculated as an initial improvement over the simple dewetting model.

Introduction

Wetting underlies practical problems ranging from insecticide spraying on leaves to soil removal by detergents.[1] Correspondingly, thin film stability has attracted a great deal of fundamental research activity.[2] In particular, the criteria for spreading a macroscopic material layer over a rigid solid substrate or a fluid surface is the same. Namely, the free energy change for spreading film A over material B is given by the spreading coefficient

$$S = \gamma_B - (\gamma_A + \gamma_{AB}) \qquad (1)$$

where γ_A and γ_B are the surface energies of A and B, respectively, and γ_{AB} is the interfacial energy between A and B. If S is positive, A prefers to spread on B. If S is negative, the contact angle for A on B is greater than zero. Thus, the A/B system could reduce its free energy by exposing the B surface to air by the nucleation and growth of holes in A. Relative to the much studied liquid/solid case, the liquid/liquid or melt/melt systems provide extra control over dewetting through the manipulation of the B viscosity η_B. For $\eta_B/\eta_A \gg 1$, the substrate acts like a solid. For $\eta_B/\eta_A \ll 1$, new complexities are introduced because the substrate can be deformed and viscous dissipation in the substrate influences dewetting. We report here optical microscopy and atomic force microscopy studies of an A polymer melt deposited on an immiscible B polymer where $\eta_B/\eta_A = 0.1$.

In the case of a liquid (melt) dewetting from a rigid solid, capillary waves on the liquid surface are thought to nucleate holes which then grow by pushing material into the rim.[3,4] If the pressure is uniform (hydrostatic equilibrium), the rim cross section is the arc of a circle with a dynamic contact angle θ_d at the solid/liquid interface. This assumption about rim shape underlies many theoretical predictions, although the rim profile has not been fully characterized. Many dewetting studies on solid substrates have been carried out.[5−9] In general, holes were found grow linearly with time, and at long times they impinged on their neighbors to form cellular patterns of droplets. The hole velocity was found to depend on film thickness and substrate type. Yerushalmi-Rozen and Klein found that the dewetting of an oligomer film from silicon is retarded by grafting a polymer brush to the substrate and adding high molecular weight polymers to the film.[10,11] In related studies, the areal density of grafted molecules was shown to control the dewetting velocity.[12] At very high grafting densities, dewetting of a film of chemically identical molecules was enhanced due to entropic repulsion.[13]

Polymer/polymer (or liquid/liquid) dewetting has received relatively little experimental attention. For thick poly(dimethylsiloxane) (PDMS) films (50−1000 μm) deposited on a bulk substrate of fluorinated PDMS, Martin *et al.*[14] observed that holes grew at a constant velocity which varied inversely with substrate viscosity and PDMS thickness. For polystyrene (91−124 nm) on poly(methyl

[†] Department of Materials Science and Engineering and Laboratory for Research on the Structure of Matter.

[‡] Department of Mechanical Engineering and Applied Mechanics.

(1) Adamson, A. W. *Physical Chemistry of Surfaces*, 5th ed.; John Wiley & Sons, Inc.: New York, 1990.
(2) deGennes, P. G. *Rev. Mod. Phys.* **1985**, *57*, 827.
(3) Brochard-Wyart, F.; Daillant, J. *Can. J. Phys.* **1990**, *68*, 1084.
(4) Safran, S. A.; Klein, J. J. *Phys. II* **1993**, *3*, 749.
(5) Reiter, G. *Phys. Rev. Lett.* **1992**, *68*, 75.
(6) Reiter, G. *Langmuir* **1993**, *9*, 1344.
(7) Sharma, A.; Reiter, G. *J. Colloid Interface Sci.* **1996**, *178*, 383.
(8) Shull, K. R.; Karis, T. E. *Langmuir* **1994**, *10*, 334.
(9) Zhao, W.; Rafailovich, M. H.; Sokolov, J.; Fetters, L. J.; Plano, R.; Sanyal, M. K.; Sinha, S. K.; Sauer, B. B. *Phys. Rev. Lett.* **1993**, *70*, 1453.
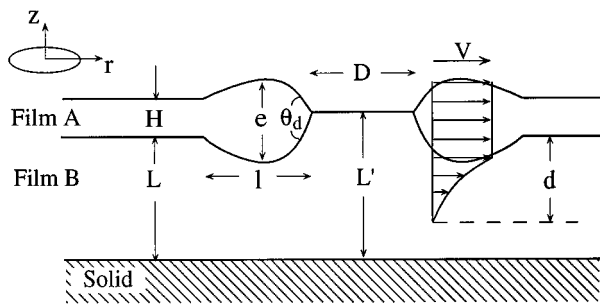(10) Yerushalmi-Rozen, R.; Klein, J.; Fetters, L. J. *Science* **1994**, *263*, 793.
(11) Yerushalmi-Rozen, R.; Klein, J.; Fetters, L. J. *Langmuir* **1995**, *11*, 2806.
(12) Reiter, G.; Schultz, J.; Auroy, P.; Auvray, L. *Europhys. Lett.* **1996**, *33*, 29.
(13) Reiter, G.; Auroy, P.; Auvray, L. *Macromolecules* **1996**, *29*, 2150.
(14) Martin, P.; Buguin, A.; Brochard-Wyart, F. *Europhys. Lett.* **1994**, *28*, 421.

Figure 1. Schematic showing a hole cross section during liquid/liquid dewetting. *H, L,* and *L'* are the unperturbed top and bottom film thicknesses, and the bottom film thickness inside the hole, respectively. *D* is the hole diameter. The rim height and width are *e* and *l*, respectively. *V* is the average rim velocity. The arrows represent the velocity field inside and under the rim. The dissipation depth of the velocity field in the bottom film is *d. z* and *r* represent the coordinate system used to calculate the height of the hole floor (eq 13) and the rim velocity profile (eq 15).

methacrylate) (PMMA) (95 nm), the dewetting velocity was found to exhibit a minimum as a function of PMMA viscosity.[15] At low PMMA viscosities, atomic force microscopy (AFM) showed that PMMA was pulled into the rim and its thickness just inside the rim was depressed. As discussed later in this paper, we believe that this lowering of the hole in polymer/polymer dewetting is due to dynamic pressure. Furthermore, the transmission electron microscopy (TEM) study presented in this paper will demonstrate why AFM must be used with care when investigating the contact line region. In a recent innovation, friction force and elastic microscopy techniques were shown to be useful methods for imaging the morphology in polymer bilayers.[16] Previously, we observed that bisphenol-A polycarbonate (PC) thin films (0.2 μm) dewet from poly(styrene-*co*-acrylonitrile) (SAN).[17] The morphology of an isolated hole was studied using a battery of techniques, including electron microscopy, atomic force microscopy, and Auger electron spectroscopy. One surprising result, revisited in this work, is the thinning of the underlying SAN layer. Preliminary studies of the hole velocity as a function of acrylonitrile (AN) content showed a minimum velocity at 0.27 weight fraction of SAN.[18] A forthcoming publication will focus on the role of interfacial width in these dewetting studies.[19]

Brochard-Wyart, Martin, and Redon (BWMR) provide a framework for describing the dewetting of liquid A from an immiscible, nonwettable, liquid substrate B.[20] The BWMR model builds upon concepts developed by Joanny[21] for describing the spreading of liquid A on an immiscible liquid substrate B. For a metastable liquid A layer (*S* < 0), holes of radius *R* (=D/2) form and the A material removed from the hole is collected in the rim. Figure 1 shows that the rim cross section is similar to a liquid lens floating on a deformable substrate. The unperturbed thicknesses of A and B are denoted as H and L, respectively. The rim size, defined by its height *e* and width *l*, is governed by conservation of mass and the dynamic contact angle θ_d at the three-phase contact line.

(15) Lambooy, P.; Phelan, K. C.; Haugg, O.; Krausch, G. *Phys. Rev. Lett.* **1996**, *76*, 1110.
(16) Overney, R. M.; Leta, D. P.; Fetters, L. J.; Liu, Y.; Rafailovich, M. H.; Sokolov, J. *J. Vac. Sci. Technol. B* **1996**, *14*, 1276.
(17) Faldi, A.; Composto, R. J.; Winey, K. I. *Langmuir* **1995**, *11*, 4855.
(18) Faldi, A.; Winey, K. I.; Composto, R. J. *Mater. Res. Soc. Symp. Proc.* **1995**, *366*, 71.
(19) Faldi, A.; Composto, R. J. Submitted for publication in *Langmuir*.
(20) Brochard-Wyart, F.; Martin, P.; Redon, C. *Langmuir* **1993**, *9*, 3682.
(21) Joanny, J. F. *Physco Chem. Hydrodyn.* **1987**, *9*, 183.

The rim experiences a net force because θ_d will generally be less than the equilibrium value θ_E defined by the Neuman triangle. In the BWMR model, the equilibrium height of liquid B inside the hole *L'* must be larger than *L* in order to equilibrate hydrostatic pressure. In our experiments, we find that *L'* is actually **less** than *L*. This observation will be explained by the dynamic pressure induced by the moving rim.

The rate of dewetting depends on the force per unit length acting on the rim. This driving force is given by the capillary and gravitational (hydrostatic) terms

$$F_d = -S - \frac{1}{2}\rho g e^2 \qquad (2)$$

where *g* and $\rho = \rho_A(\rho_B - \rho_A)/\rho_B$ are the gravity and effective density, respectively. In our experiments, the gravity contribution is ~10^{-6} and can be ignored. As the rim slides over a bulk substrate B, a frictional force proportional to the rim velocity *V* is induced by the viscous stress at the A/B interface. Following the scaling description of BMWR

$$F_f \sim \eta_B V \qquad (3)$$

where η_B is the zero shear-rate viscosity of B. The motion of the rim is controlled by balancing the driving and frictional forces ($F_d = F_f$)

$$V = \frac{|S|}{\eta_B} = \left(\frac{\gamma}{\eta_B}\right)\theta_E{}^2 \qquad (4)$$

where the gravitational term is neglected. Equation 4 predicts that the hole opening velocity is constant and independent of A and B thicknesses. For the case of liquid A dewetting from a thick, viscous B film, the viscous flow penetrates into the B layer and dissipates within a depth *d* as shown in Figure 1. Note that a homogeneous flow in the rim is assumed in this model. As shown later, a nonhomogeneous flow results from the shape of the rim determined by AFM.

The BWMR model also describes the dewetting of liquid A from a substrate B having a finite thickness *L*. For *L* ≫ *d*, the damping of the viscous flow in B is not disturbed by the solid surface under B. But if *L* < *d*, the viscous flow near the solid surface is expected to be zero. This "no slippage" condition can be due to a glassy polymer layer or grafted polymer chains.[22] Under no-slip conditions, the frictional force is inversely related to the thickness of B

$$F_f = 4\eta_B\left(\frac{l}{L}\right)V \qquad (5)$$

where the rim width $l = 2(HR/\theta_d)^{1/2}$ is determined from mass conservation of A. Upon balancing F_d and F_f, the hole velocity is given by

$$V = \theta_E{}^{1/3}\left(\frac{\gamma_B}{\eta_B}\right)^{2/3}\left(\frac{L^2}{H}\right)^{1/3} t^{-1/3} \qquad (6)$$

Equation 6 predicts that the hole opening velocity decreases as the hole grows. Moreover, the hole velocity is expected to increase as the B thickness increases and A thickness decreases. These predictions will be compared with our experiment results on the PC/SAN system.

In the BWMR model, analytic expressions for the hole velocity are found only after making several assumptions. Before experimental results are compared with the BWMR model, these assumptions are briefly reviewed. First, by using a hemispherical rim shape, the pressure inside the rim is assumed to be at equilibrium during dewetting.

(22) Brochard-Wyart, F.; deGennes, P. G. *Langmuir* **1992**, *8*, 3033.

Table 1. Characteristics of PC and SAN

polymers	M_w	M_w/M_n	ρ (g/cm³)	source
PC	19 100	2.94	1.08	General Electric
SAN	118 000	2.24	1.07	Monsanto

Also, L' is found to be greater than L because of the difference in hydrostatic pressure on the B layer inside and outside the hole. Both pressure requirements may not be valid if viscous flow occurs in the rim or substrate. Later, we will present results showing that the shape of the rim is asymmetric and that L' is actually less than L. A new model will be presented in the discussion section to address this latter observation. Second, the BWMR model assumes that the entire rim moves with a uniform velocity V independent of the radial and vertical positions. However, a velocity gradient at the A/B interface would produce a shear stress gradient and as a result a nonuniform rim velocity. Thus, the viscous frictional forces given by eqs 3 and 5 would need modification. Third, the BWMR model neglects viscous dissipation within the rim. For $\eta_A > \eta_B$, this viscous dissipation should be important and cause the rim top to have a larger velocity than at the A/B interface. Including the nonuniform rim velocity and viscous damping in A would effectively reduce the frictional force acting on the rim. Using the measured rim shape, we have expanded upon the BWMR model by numerically solving for the rim velocity profile. Fourth, the A/B interface under the rim is taken to be flat. Recent experiments show that this interface can be curved.[15,23] With these assumptions in mind, the BWMR model still provides an important guide for understanding polymer/polymer dewetting.

In this paper, we will explore the kinetics and morphology of polymer/polymer dewetting where A and B correspond to bisphenol-A polycarbonate (PC) and poly-(styrene-*co*-acrylonitrile), respectively. Previous studies of PC (200 nm) films on SAN (200 nm) focused on the morphology of polymer/polymer dewetting.[17] In this study, the hole opening velocity and rim shape are studied as a function of the PC and SAN film thicknesses. These experimental results are compared with predictions based on the BWMR model.

Experimental Section

Immiscible polymer bilayers, A/B, were prepared from bisphenol-A polycarbonate (PC or A) and poly(styrene-*co*-acrylonitrile) (SAN or B) with an acrylonitrile weight fraction of 0.33. The polymer characteristics are shown in Table 1. PC and SAN were dissolved in methylene chloride and chloroform, respectively, and precipitated using methanol to remove oligomers and impurities. This precipitation procedure was performed three times.

The glass transition temperatures (T_g) and zero-shear viscosities (η_0) of the purified polymers were measured. Using a Perkin-Elmer DSC7 differential scanning calorimeter, PC and SAN samples were heated from 70 to 200 °C at a heating rate 20 °C/min. The measured T_g values were 153 and 115 °C for PC and SAN, respectively. The zero shear viscosities of PC and SAN at 180 °C were measured on a Rheometrics Solids Analyzer II in a shear sandwich geometry. Linear oscillatory shearing was applied to the polymer samples to measure the dynamic viscosity as a function of shear rate. The Carreau model[24] was used to analyze the data and determine η_0. The zero shear viscosities of PC and SAN were $\eta_{0,PC} = 1.92 \times 10^7$ and $\eta_{0,SAN} = 1.36 \times 10^6$ P, respectively. Thus, the top PC film is about 10 times more viscous than the underlying SAN substrate film. This ratio of $\eta_{0,PC}/\eta_{0,SAN}$ should be large enough to satisfy the

condition for plug flow inside the rim, $\eta_{0,SAN} < \eta_{0,PC}/\theta_E$.[25] The dynamic viscosity measurements also provide information about the shear rates that produce shear thinning.[24] For both PC and SAN, the dynamic viscosities decrease moderately above 0.01 s⁻¹ and more rapidly for shear rates greater than 0.1 s⁻¹. Thus, shear thinning of the PC or SAN layer can occur at very rapid hole velocities.

The PC/SAN bilayer is supported by a Si(100) wafer which is covered by a native oxide. The SAN film was spin-coated directly onto the Si wafer from a methyl isobutyl ketone solution and dried at 70 °C for at least 12 h under vacuum. The SAN thickness was measured by ellipsometry. The PC film was spin-coated onto a clean glass slide from a tetrachloroethane solution, floated off the slide onto a water bath, and then picked up from underneath with a SAN/Si sample. The PC/SAN/Si sample was then dried at 70 °C for at least 12 h under vacuum. The PC layer thickness was also measured by ellipsometry. Refractive indices of 1.575 and 1.585 for SAN and PC, respectively, were used for the ellipsometry measurements. PC film thicknesses of 200 nm and 310 nm were studied. These PC layers were deposited on SAN films of various thicknesses in order to prepare a series of samples denoted as PC200 and PC310, respectively. The SAN thickness was controlled by either varying the solution concentration (1.5−8.0 wt %) or stacking films having the same thickness. For both the PC200 and PC310 series, the SAN film thicknesses were 50, 125, 260, 400, 540, and 1850 nm.

The PC/SAN samples were annealed in a Mettler FP90 hot stage held at 180 °C. The temperature was calibrated from the melting temperatures of benzophenone and benzoic acid (Mettler ME-18870 and ME-18555, respectively). The dewetting process was viewed under a Leitz Laborlux optical microscope in reflection geometry and recorded by a video recording system or 35 mm film. After the bilayers were held at 180 °C for an initial period, holes in the metastable PC layer became observable and continued to grow. The diameters of several isolated holes in each sample were recorded as a function of time. The smallest hole diameter that could be imaged (~10 μm) was determined by the microscope magnification, which was kept constant. One objective of this study was to observe the growth of isolated holes; thus, the nucleation density provided a constraint on the largest hole diameters that could be measured (~150 μm). After neighboring holes impinged, the bilayer was quenched to room temperature, which is below the T_g of both PC and SAN. The "quenched" hole morphology was then studied by atomic force microscopy.

Using a Digital Instrument NanoScope III, AFM images of the holes were taken under ambient conditions in contact mode with a silicon tip. A scan rate of 50−100 Hz was used. To check for sample damage due to the tip, images were obtained by scanning across one hole from left to right and then from right to left. These images were indistinguishable in all cases.

Results

Dewetting in the PC200 Series. Figure 2 shows an optical micrograph (OM) of the top view of holes in a PC(200 nm)/SAN(260 nm) sample annealed at 180 °C for 150 min. An isolated hole is observed near the center of the micrograph. This hole is circular and is surrounded by a rim. The hole diameter D is defined by the inside of the dark ring and is 51 ± 1 μm for this particular hole. As shown later, the floor of the hole (light gray) is flat except near the center (dark dot), which is depressed. The region between holes (medium gray) corresponds to flat, unperturbed PC/SAN layers on a rigid substrate. In the lower right corner of the micrograph, two holes have collided and are separated by a ridge. Note that these holes are no longer circular. This paper will focus on the growth and morphology of isolated holes.

Figure 3 shows the hole diameter as a function of annealing time, t, for PC200/SAN(L) at 180 °C. The SAN thickness, L, increases from 125 to 1850 nm. The error bars for D are determined from measurements on several

(23) Winey, K. I.; Faldi, A.; Composto, R. J. In *Microscopy and Microanalysis*; Jones and Begell: Cincinnati, OH, 1995; p 182.

(24) Bird, R. B.; Armstrong, R. C.; Hassager, O. *Dynamics of Polymeric Liquids: Fluid Mechanics*; John Wiley & Sons, Inc.: New York, 1977.

(25) The equilibrium contact angle is expected to be ~1 radian or less in our system.
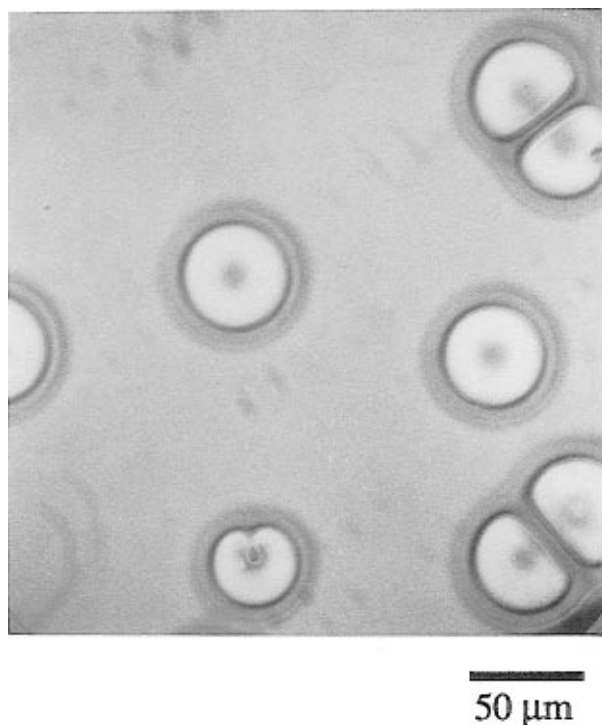
Figure 2. Optical micrograph of holes in PC(200 nm)/SAN(260 nm) bilayer after annealing for 150 min at 180 °C. The dark gray circles denote the inside of the rim. The medium gray circles in the center of each hole correspond to depressions (see Figure 5b). Both isolated and impinging holes are shown.
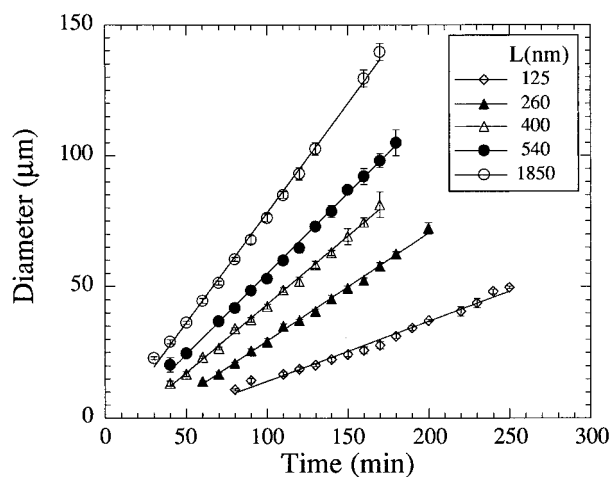

Figure 3. Hole diameter versus time for the PC200 samples annealed at 180 °C. Error bars are discussed in the text. The lines are linear fits to the data which give the hole velocities as plotted in Figure 4.

different holes. Over the experimentally accessible range of D, the hole diameter is found to grow linearly with time for all SAN thicknesses studied. Note that eq 6 predicts that hole growth should slow down, $D \sim t^{2/3}$. One possible explanation may be the difference between the model and experimental hole topography, as discussed later.

The hole velocity, $\mathrm{d}(D/2)/\mathrm{d}t$, as a function of L is shown in Figure 4. The hole velocity increases as the bottom film thickness increases. For film thicknesses less than the dissipation depth, d, this result is expected because the energy produced by the moving rim can be dissipated more effectively as the bottom film thickness increases. As a result, the frictional drag on the rim decreases. As L increases from 125 to 540 nm, the hole opening velocity for the PC200 series increases linearly with L, $V \sim L$. Note that this scaling relationship is stronger than that
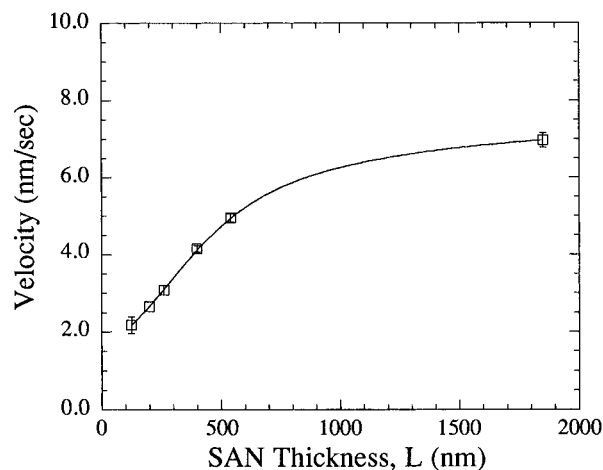

Figure 4. Hole velocity as a function of SAN layer thickness L for the PC200 samples. The annealing temperature is 180 °C. The solid line is to guide the eye. The velocity becomes relatively independent of L for $L > 1000$ nm, which corresponds to the dissipation depth.
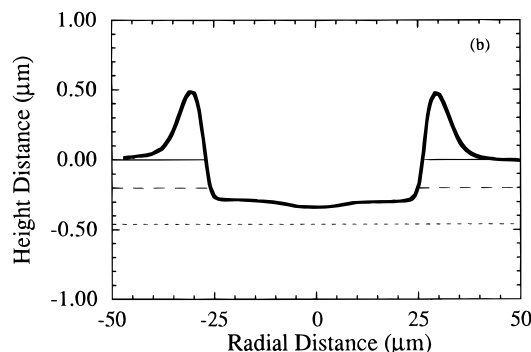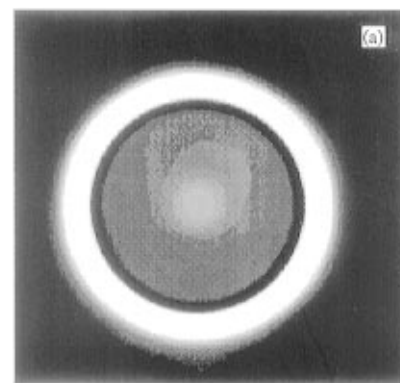
Figure 5. AFM images of a hole in PC(200 nm)/SAN(260 nm) annealed at 180 °C are shown in a (a) top view and (b) line profile. In part b, the thin solid, long-dashed, and dotted lines correspond to the original PC surface, the original PC/SAN interface, and the SAN/Si interface, respectively.

in the BWMR model (eq 6) where $V \sim L^{2/3}$. As L continues to increase, the velocity increases much more slowly beyond $L \sim 1000$ nm. Thus, in PC/SAN the SAN behaves as a "bulk" substrate for thicknesses greater than $\sim 1 \mu m$. These results represent the first study of the influence of bottom film thickness on polymer/polymer dewetting.

The hole morphology was observed by atomic force microscopy (AFM). Figure 5 shows an AFM image of an isolated hole in PC(200 nm)/SAN(260 nm). This hole diameter is 50.4 μm and is therefore similar in size to the one shown in Figure 2. The contour map image in Figure 5a shows that the hole is surrounded by a circular rim (bright white ring), relatively flat inside this rim (uniform gray) and depressed in the center (light disk). These
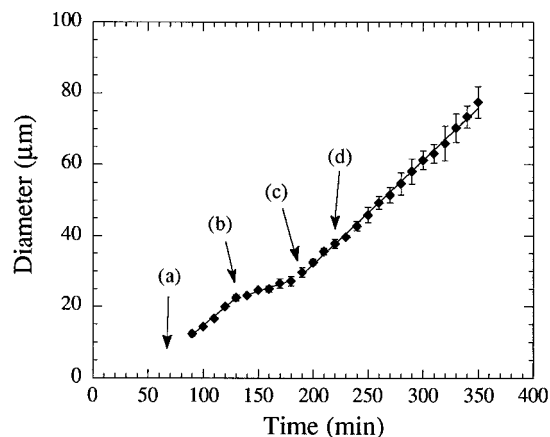
Figure 6. Hole diameter, *D*, versus time for PC(200 nm)/SAN(50 nm) annealed at 180 °C. Arrows (a), (b), (c), and (d) correspond to the AFM profiles shown in Figure 7. The solid lines are fits to the data at early, intermediate, and late stages of growth. The late stage hole velocity is 2.1 nm/s.

features are consistent with the OM observations shown in Figure 2. Figure 5b shows a height profile across the center of the hole. This line profile demonstrates that the hole floor is relatively flat except for a shallow dimple about 30.0 nm deep and 21.3 μm wide near the center ($r = 0$). The rim shape is asymmetric with a steep slope on the inside and a more gradual slope on the outside. For this hole, the rim is ~0.5 μm high relative to the unperturbed PC surface ($z = 0$) and has a full-width at half maximum (fwhm) of 6.4 μm. An important observation which impacts the applicability of applying the BWMR model to PC/SAN dewetting is that the hole floor is about 130 nm **lower** than the original PC/SAN interface (long dashed lines). These morphological features are consistent with our previous studies.[17,18]

To further examine the influence of bottom film thickness, dewetting studies were carried out on bilayer samples having an ultrathin SAN thickness of 50 nm, about 3 times the SAN radius of gyration. Figure 6 shows the hole diameter as a function of time for PC(200 nm)/SAN(50 nm) at 180 °C. In contrast to the linear growth observed for thicker SAN layers (Figure 3), in the ultrathin SAN case the holes grow linearly with time at first, then much more slowly, and finally linearly again with a velocity similar to the initial one. One way to understand this new behavior is to complement the hole velocity measurements with studies of the morphology during each stage of growth.

To this end, AFM images of PC(200 nm)/SAN(50 nm) samples were taken during (a) hole nucleation, (b) the beginning of intermediate stage growth, (c) the beginning of late stage growth, and (d) late stage growth. These holes are denoted as (a), (b), (c), and (d) in Figure 6. The corresponding AFM line profiles are shown in parts a–d of Figure 7, respectively. In Figure 7, the original PC surface, original PC/SAN interface (long-dashed line), and SAN/Si interface (dotted line) are located at $z = 0$, -0.20 μm, and -0.25 μm, respectively. During the early stage of growth represented in Figure 7a, a depression in the PC develops to a depth of ~100 nm beneath the original PC surface. This depression has not yet reached the PC/SAN interface and is growing in both depth and width. Note that the rim is quite low. At the beginning of the intermediate stage (Figure 7b), a hole in the PC layer has formed with a well-defined diameter of 22.5 μm. The hole floor is now flat and has a very shallow dimple at the center. Compared with Figure 7a, the rim is much larger, having a height and fwhm of about 0.3 and 3.5 μm, respectively. Note that the rim shape is asymmetric, in

agreement with Figure 5 and previous studies.[17] The hole depth of 230 nm is only slightly less than the total bilayer thickness of 250 nm. This observation suggests that SAN is pulled into the rim during dewetting and a thinner SAN layer is left on the Si surface.

During the intermediate stage, the hole velocity is twice as slow as during the initial stage of growth (see Figure 6). This slowing down can be understood by comparing parts b and c of Figure 7. Whereas the hole diameter increases from 22.5 to 30 μm, the hole depth does not change over this time period (i.e., from 130 to 190 min). Thus, during the intermediate stage dewetting is no longer between two polymer layers but rather between a polymer film and bound SAN chains. After this slow period of growth, the hole diameter again increases more rapidly. Parts c and d of Figure 7 display hole profiles during the late stage of growth. During this period, the hole diameter increases from 30.0 to 37.5 μm, the hole depth remains unchanged, and the dimple in the hole floor becomes less pronounced. The hole diameter grows linearly with time and has a velocity of 2.1 nm/s. A detailed analysis of the AFM image near the three-phase contact line shows that the "topological" dynamic contact angle is smaller during the late stage of growth compared with the intermediate stage. This rearrangement of the contact angle results in an increase in the driving force for dewetting and may account for the transition between intermediate and late stage growth. As shown later, AFM may provide misleading information about the dynamic contact angle, and therefore an unambiguous analysis demands cross-sectional images of the rim. The initial and late stage velocities appear similar. This result was unexpected because the initial and late stages correspond to dewetting at the melt/melt and melt/bound layer interfaces, respectively. Further measurements must be taken during the initial stage of growth before making any conclusions.

Dewetting in PC310 Series. Thus far, the dewetting kinetics and morphology of PC(H)/SAN(L) bilayers were studied at constant *H* (200 nm) as the bottom film thickness was varied from relatively thick, 1850 nm, to very thin, 50 nm. In qualitative agreement with the BWMR model, holes grew more slowly as *L* decreased for $L < 1000$ nm. Correspondingly, hole growth should also be suppressed upon increasing the PC layer thickness. This prediction will be tested next. Figure 8 shows the hole diameter as a function of time for the PC310 samples, namely, PC(310 nm)/SAN(*L*), at 180 °C. In qualitative agreement with the PC200 results, the hole diameter increases more rapidly as the SAN layer thickness increases. However, in contrast to the PC200 results, the hole diameter does not grow linearly with time. Rather, the hole diameter increases as $D \sim t^{\alpha}$, where the exponent α increases from 1.1 to 1.6 as *L* decreases from 1850 to 125 nm, respectively. Thus, hole acceleration becomes more pronounced as the SAN layer decreases. To the best of our knowledge, hole acceleration has not been previously observed for either polymeric or liquid systems.

The hole velocity as a function of SAN thickness is shown in Figure 9 for the PC310 series. Because the velocity increases with time, the velocities are compared at the same hole diameter. For example, the open squares represent the velocity of a 30 μm hole, whereas the closed squares represent a 150 μm hole. Note, that at constant *L*, the hole velocity increases by a factor of up to 2 as *D* increases by a factor of 5, from 30 to 150 μm. This observation simply reflects the hole acceleration. For each *D*, the hole velocity increases with *L* and approaches a plateau at large *L*, in qualitative agreement with the PC200 case. For $D < 50$ μm, the hole velocities for the
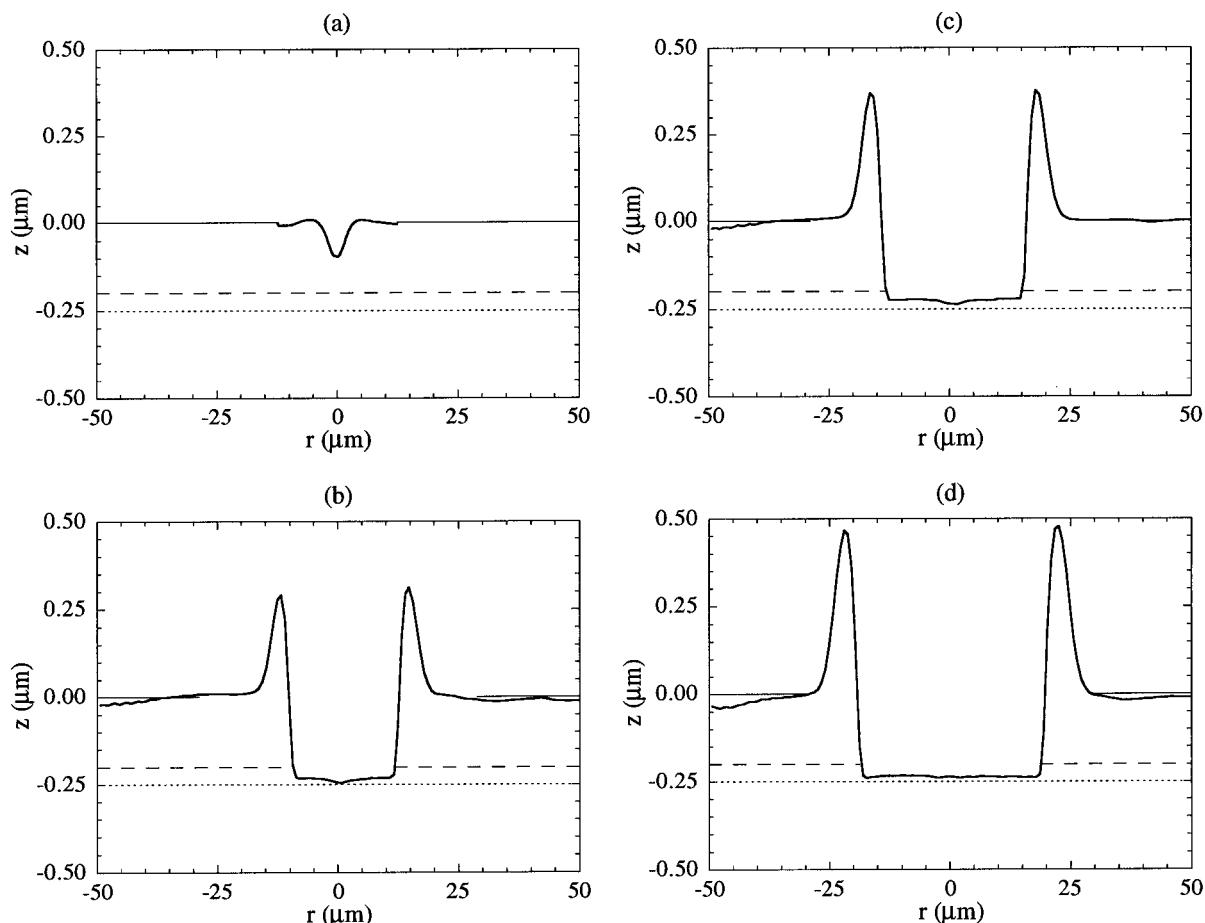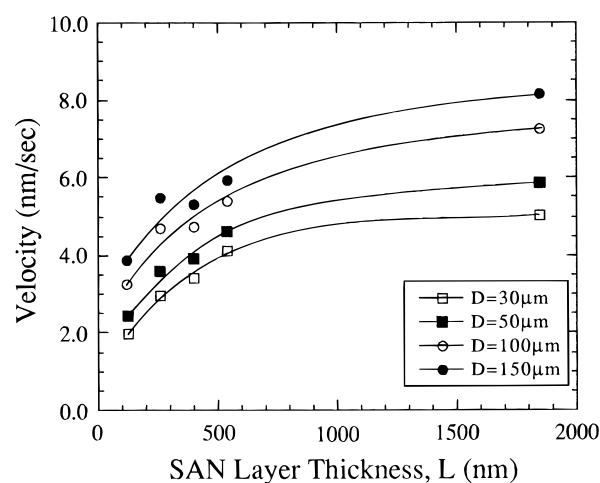
Figure 7. Line profiles of holes in PC(200 nm)/SAN(50 nm) shown at (a) 70, (b) 130, (c) 190, and (d) 220 min. The hole sizes in parts b−d are 22.5, 30.0, and 37.5 μm, respectively. The original PC surface, the original PC/SAN interface (long-dashed line), and the SAN/Si interface (dotted line) are located at $z = 0$, -0.20, and -0.25 μm, respectively.
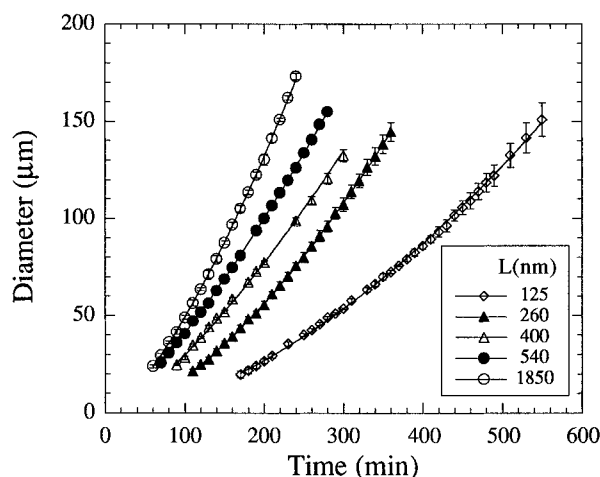
Figure 8. Hole diameter versus time for PC310 samples at 180 °C. Error bars are discussed in the text. The solid lines represent best fits of $D \sim t^{\alpha}$, where α increases from 1.1 to 1.6 as L decreases from 1850 to 125 nm. The hole velocities are plotted in Figure 9.

Figure 9. Hole velocity as a function of SAN layer thickness L for PC310 samples at 180 °C. Because of hole acceleration, velocities are compared at constant hole diameters. Solid lines are a guide to the eye.

PC310 samples are smaller than those in PC200. This result indicates that an increase in the PC layer thickness suppresses hole growth, in qualitative agreement with eq 6. However, because of acceleration, large holes (i.e., $D > 50 \mu$m) grow at a faster rate than in the PC200 series. In contrast to BWMR predictions and recent experiments,[14] this observation suggests that increasing the top layer thickness can enhance, rather than retard, hole growth. Further studies are necessary before the effect of PC layer thickness on dewetting is understood.

Discussion

For the PC200 series, the hole velocity is constant with time for each SAN thickness. This result is in agreement with dewetting studies of thick (50 μm to 1 mm) poly(dimethylsiloxane) (PDMS) films on bulk fluorinated PDMS substrates.[14] However, for the PC310 series the hole velocity clearly increases with time. One possible explanation is that the shear thinning effect of the SAN layer aggravates the acceleration of the hole growth. Using data from Figure 9, the shear rates ($\epsilon \sim V/L$) range from

Figure 10. Cross-sectional TEM image of a rim in PC(200 nm)/SAN(200 nm). From bottom to top, the image shows the polyimide substrate, gold marker layer (black), SAN layer (light gray), and PC layer (dark gray). The PC layer was stained using ruthenium tetraoxide solution. The dynamic contact angle of 140° is defined with respect to the three-phase contact line at the air, PC, and SAN interface.

0.01 to 0.1 s^{-1}. These rates cover a range where the SAN viscosity just starts to decrease rapidly with shear rate. As viscosity decreases, the rim accelerates because the frictional force on the rim is now smaller. Eventually, a terminal velocity is reached and the frictional force is balanced by the capillary force.

If shear thinning causes acceleration in the PC310 series, one might expect the holes in the PC200 series to also grow with an increasing velocity. However, as shown in Figure 3, the hole velocity in PC200 is constant over the measured range. One possible explanation for this apparent contradiction is that the terminal velocity is reached more quickly in PC200. Measuring D over a wider range of sizes would improve the sensitivity for observing hole acceleration. However, the high hole density in PC200 limits the size of the largest isolated holes that can be measured. This observation is in good agreement with dewetting experiments of polystyrene (PS) on silicon where the nucleation density increased as the PS thickness decreased.[5] An alternative interpretation by Brochard Wyart[30] suggests that hole acceleration may reflect a change in the dominate dissipation mechanism during hole growth. Initially, hole growth is dictated by dissipation in the bottom film, whereas at later times, when the rim is high, dissipation within the rim dominates. The crossover time between mechanisms should increase with bottom film thickness. We plan to test this suggestion by varying the PC thickness over a wide range.

An increase in the capillary potential energy can also cause acceleration. Taking the rim as part of a lens (see Figure 1), the dewetting force is $\gamma_A[\cos \theta_e - \cos \theta_d(t)]$, where the dynamic contact angle θ_d is less than the equilibrium contact angle θ_e. Shanahan and Carre[26-28] have shown that the spreading velocity of liquids on rubbers slows down because θ_d approaches θ_e. This viscoelastic breaking is attributed to the viscoelastic dissipation of energy resulting from the deformation of the substrate caused by the vertical component of the surface tension at the three-phase contact line. Similarly, if $\theta_d(t)$ decreases during polymer/polymer dewetting, the driving force for dewetting will increase leading to acceleration.

To test this hypothesis, cross-sectional transmission electron microscopy was used to image the three-phase contact line to determine the dynamic contact angle. Technique details were given previously.[23] Figure 10 shows the rim consisting of a PC layer (dark) over the SAN layer (light). A gold-coated polyimide substrate was used instead of Si to permit microtomy in order to prepare cross sections of the bilayer. The main observation is that the actual shape of the PC layer differs greatly from the lens geometry depicted in Figure 1. The PC retracts into the rim during dewetting. Moreover, the SAN is pulled up into the rim. Thus, the vertical component of the surface tension indeed appears to deform the bottom layer. This elevation of the contact line was also recently observed by Lambooy *et al.*[15] For the "snap shot" shown in Figure 10 the dynamic contact angle is approximately 140°. Due to its complexity, this dynamic contact angle could not be determined from AFM. Thus, AFM measurements of liquid/liquid dynamic contact angles must be employed with care. Removal of the top layer is one approach to directly image the buried interface;[15] however, the interface in Figure 10 could never be imaged in this way because of its concave shape. Further studies are needed to extract reliable dynamic contact angles and to determine if this angle is time dependent. In agreement with the AFM trace shown in Figure 5, L' is less than L. In summary, Figure 10 demonstrates that the rim shape differs significantly from the model shape given in Figure 1. Because the model shape underlies calculations made in the BWMR theory, a comparison between theoretical predications and our experimental results must be made with caution.

For both the PC200 and PC310 samples, the hole velocity appears independent of SAN thickness for L greater than ~1000 nm (Figures 4 and 9). However, this observation is not entirely conclusive due to the limited data points available. For the experiments presented here, the presence of the solid substrate will be always felt due to the small SAN layer thickness and high SAN viscosity. In fact, the calculated viscous dissipation depth of the SAN layer is ~10^5 m.[29] The transient nature of the moving rim can be safely neglected since the time for a moving rim to reach a steady state velocity profile is on the order

(26) Shanahan, M. E. R. *Langmuir* **1995**, *11*, 1041.
(27) Shanahan, M. E. R.; Carre, A. *Langmuir* **1994**, *10*, 1647.
(28) Shanahan, M. E. R.; Carre, A. *Langmuir* **1995**, *11*, 1396.
(29) White, F. M. *Viscous Fluid Flow*, 2nd ed.; McGraw-Hill, Inc.: New York, 1991.
(30) Brochard-Wyart, F. Personal communication.

of 10^{-5} s.[29] Thus, the viscous shear flow in the SAN layer should follow steady-state behavior.

The experimental (AFM and TEM) and model (Figure 1) hole morphologies differ in at least two ways. As mentioned previously, the underlying SAN layer is deformed due to the vertical component of the surface tension. This deformation is consistent with the relatively low SAN viscosity ($\eta_{0,PC}/\eta_{0,SAN} \sim 10$). Because SAN is removed from the hole, the rim collects not only PC but also SAN from the underlying film. Thus, the rim morphology does not correspond to a rim of PC receding over a flexible SAN layer as shown in Figure 1. The hole morphology is also inconsistent with hydrostatic equilibrium conditions. Namely, hydrostatic equilibrium requires that the SAN inside the hole should rise above the original PC/SAN interface. Experimentally, AFM and TEM results clearly show that L' is less than L. As discussed below, this observation may result from the pressure induced by rim motion.

The hydrostatic and dynamic pressures determine the height of the hole floor, L'. The difference in hydrostatic pressure between the inside and outside of the rim is

$$\Delta P_{hy} = (\rho_A g H + \rho_B g L) - \rho_B g L' \qquad (7)$$

In addition, the viscous flow induced by the rim motion requires a pressure gradient opposite to the rim motion to conserve mass flow in the SAN layer. For flow under the rim, the equation of motion using the coordinate system in Figure 1 is[24]

$$0 = -\frac{\partial P_B}{\partial r} + \eta_B \frac{\partial^2 u_r}{\partial z^2} \qquad (8)$$

where P_B is the radial pressure experienced by liquid B and u_r is the flow velocity radial to the hole. For the boundary conditions $u_r(z{=}0) = 0$ and $u_r(z{=}L) = V$, this flow velocity is described by

$$u_r = \frac{1}{2\eta_B} \frac{\partial P_B}{\partial r} z(z - L) + V\frac{z}{L} \qquad (9)$$

From conservation of mass, the zero flux condition in layer B is

$$\int_0^L u_r(2\pi r) \, dz = 0 \qquad (10)$$

From eqs 8–10 and neglecting the complex flow behavior near the contact line, the dynamic pressure difference ΔP_{dy} between the inside and outside of the rim is

$$\Delta P_{dy} = \frac{6\eta_B V}{L^2} l \qquad (11)$$

Note that this term must be positive. Because the hydrostatic pressure difference must balance the dynamic pressure difference, the height of the hole floor is

$$L' = L + \frac{\rho_A}{\rho_B} H - \frac{6\eta_B V l}{\rho_B g L^2} \qquad (12)$$

In eq 12, the second term acts to raise the hole height due to the hydrostatic pressure whereas the third term lowers L' below the original A/B interface because of rim motion. Note that the dynamic pressure contribution can be particularly important for highly viscous polymeric systems. Although not in quantitative agreement with our results, eq 12 partly explains why the SAN layer lowers
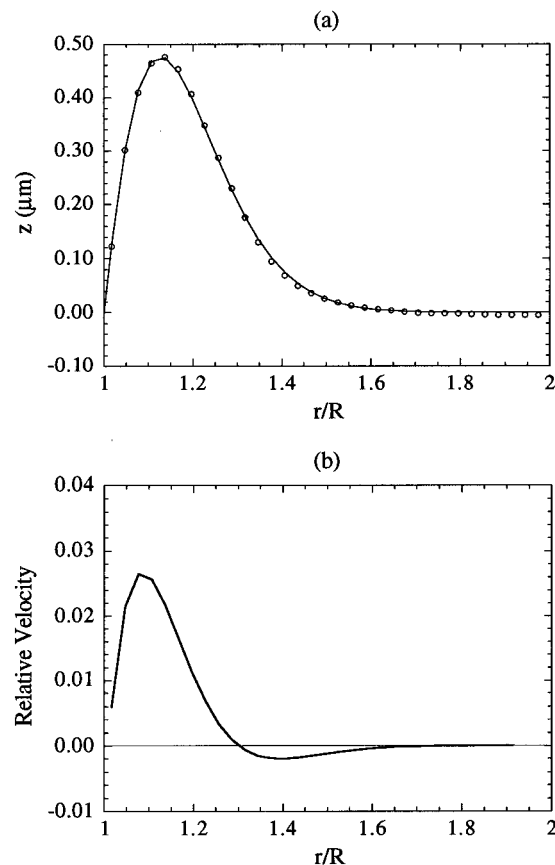
Figure 11. (a) Rim profile in PC(200 nm)/SAN(260 nm) versus reduced distance, r/R, where R is the hole radius. The open symbols and solid line correspond to the AFM profile in Figure 5b and eq 13, respectively. In eq 13 a, b, and R correspond to 7.6 μm, 13.1, and 26.1 μm, respectively. (b) The velocity distribution in the rim determined from Figure 11a and eq 15.

during dewetting. An improved model would incorporate the complex flow suggested by Figure 10. In a recent experiment on PS dewetting from PMMA, AFM results suggest that L' is the same as the original height L.[15] Clearly, further studies are needed to understand how the height of the hole floor depends on fundamental parameters.

The BWMR model assumes a homogeneous flow field inside the rim (see Figure 1). To improve upon this model, the flow field can be more accurately determined from the rim shape shown in Figure 5b. The rim height can be described by

$$h = a\left(1 - \frac{R}{r}\right) \exp\left[-b\left(\frac{r}{R} - 1\right)^{1.5}\right] \qquad (13)$$

where a and b are fitting parameters and R is the hole radius. Figure 11a shows the rim profile determined from AFM (open circles) and eq 13 (solid line). Note that the rim fwhm is 25% of the hole radius. The pressure and velocity distributions across the rim are[29]

$$P_A(r) \propto \frac{1}{r} \frac{\partial}{\partial r}\left(r \frac{\partial h}{\partial r}\right) \qquad (14)$$

and

$$v(r) \propto \frac{\partial P_A}{\partial r} \propto \frac{\partial}{\partial r}\left(\frac{1}{r} \frac{\partial}{\partial r}\left(r \frac{\partial h}{\partial r}\right)\right) \qquad (15)$$

respectively. Figure 11b shows how $v(r)$ varies with r/R. As r/R increases from 1.0, the velocity initially increases,

has a maximum value near the highest part of the rim, and then decays to small values for $r/R > 1.3$. In contrast to a uniform velocity profile, Figure 11b shows that the rim velocity is nonuniform and strongly varies with rim position. Because the velocity is essentially zero near the rim tail ($r/R > 1.3$), the rim must grow by a rolling mechanism in which material on the top of the rim is pushed into the tail region. To test this model, studies of the rim shape as a function of time are underway.

Conclusions

This study explores the dewetting of a PC melt from an underlying SAN melt as a function of top (H) and bottom (L) layer thicknesses. For a 200 nm PC layer, the hole diameter grows linearly with time at a constant velocity. The hole velocity increases linearly with SAN thickness as L increases from 125 to 540 nm and becomes nearly constant for L greater than about 1000 nm. The dewetting behavior for very thin SAN layers ($L = 50$ nm) exhibits three stages of hole growth. During the initial and final stages, holes grow at a constant velocity. This velocity is about two times that of the intermediate state. AFM studies show that the intermediate stage begins when the hole impinges on the silicon substrate. During this stage the three-phase contact line is expected to rearrange to produce a new contact angle.

Upon increasing the PC thickness to 310 nm, the hole diameter is observed to accelerate with time according to a power law dependence. Qualitatively, the hole velocities for both the PC200 and PC310 series have a similar dependence on L. A quantitative comparison between a simple liquid/liquid model prediction and our results is problematic because of the complexity of the hole morphology. TEM studies show that the three-phase contact line between PC, SAN, and air is nonplanar and has a significant vertical component. TEM and AFM experiments show that SAN from the underlying layer is pulled into the rim during dewetting. The resulting decrease in SAN thickness was explained by considering the hydrostatic and dynamic pressure acting on the hole. Using the rim topography generated by AFM, the velocity profile inside the rim was calculated. This velocity was found to be a maximum near the highest rim section and to decay monotonically away from the hole. This observation suggests that the rim grows by a rolling mechanism in which material is taken from the top of the rim and pushed into the tail region. These experimental and theoretical results should provide both the incentive and guidance for future investigations of dewetting at the polymer/polymer interface.

LA960757X